5-2012

Hybrid Carbon-Based Scaffolds for Applications in Soft Tissue Reconstruction

Jarema S. Czarnecki

Khalid Lafdi

Robert M. Joseph
University of Dayton, rjoseph2@udayton.edu

Panagiotis A. Tsonis
University of Dayton, ptsonis1@udayton.edu

TISSUE ENGINEERING: Part A
Volume 18, Numbers 9 and 10, 2012

DOI: 10.1089/ten.tea.2011.0533

Hybrid Carbon-Based Scaffolds for Applications in Soft Tissue Reconstruction

Jarema S. Czarnecki, M.S.,[1,2] Khalid Lafdi, D.Sc., Ph.D.,[1,3,4] Robert M. Joseph, D.P.M., Ph.D.,[3,5] and Panagiotis A. Tsonis, Ph.D.[3,6]

Current biomedical scaffolds utilized in surgery to repair soft tissues commonly fail to meet the optimal combination of biomechanical and tissue regenerative properties. Carbon is a scaffold alternative that potentially optimizes the balance between mechanical strength, durability, and function as a cell and biologics delivery vehicle that is necessary to restore tissue function while promoting tissue repair. The goals of this study were to investigate the feasibility of fabricating hybrid fibrous carbon scaffolds modified with biopolymer, polycaprolactone and to analyze their mechanical properties and ability to support cell growth and proliferation. Environmental scanning electron microscopy, micro-computed tomography, and cell adhesion and cell proliferation studies were utilized to test scaffold suitability as a cell delivery vehicle. Mechanical properties were tested to examine load failure and elastic modulus. Results were compared to an acellular dermal matrix scaffold control (GraftJacket® [GJ] Matrix), selected for its common use in surgery for the repair of soft tissues. Results indicated that carbon scaffolds exhibited similar mechanical maximums and capacity to support fibroblast adhesion and proliferation in comparison with GJ. Fibroblast adhesion and proliferation was collinear with carbon fiber orientation in regions of sparsely distributed fibers and occurred in clusters in regions of higher fiber density and low porosity. Overall, fibroblast adhesion and proliferation was greatest in lower porosity carbon scaffolds with highly aligned fibers. Stepwise multivariate regression showed that the variability in maximum load of carbon scaffolds and controls were dependent on unique and separate sets of parameters. These finding suggested that there were significant differences in the functional implications of scaffold design and material properties between carbon and dermis derived scaffolds that affect scaffold utility as a tissue replacement construct.

Introduction

Autologous grafts have been the "gold standard" in tissue replacement and the most accurate means of recapitulating both the biologic and mechanical properties of tissue. However, autologous grafts have had complications and drawbacks. Skin grafting, a prime example of an autologous tissue graft, has been limited by the size of graft, availability, and secondary donor site morbidity.[1] Use of cadaveric tissues circumvents several limitations of autologous grafts, however, sterilization processes used to reduce the risk of disease transmission potentially weaken tissues and eliminates living cells and some growth factors from scaffolds to make them suboptimal tissue replacements.[2,3] Chemical cross-linkage of tissue scaffolds has been employed in some circumstances to strengthen weak tissues but can result in a prolonged inflammatory response and limit graft integration *in vivo*.[4–9] Partial enzymatic digestion of cadaveric tissues has also been utilized to improve graft porosity, which potentially assists with graft neovascularization, however, this procedure has not been overwhelmingly successful.[8] Proprietary methods of chemically and physically stripping tissues of cellular materials have been commercially developed to minimize graft rejection and loss of essential biologic factors; however, these methods cannot be universally applied to all tissues.[6,10] GraftJacket® Matrix (Wright Medical),[4] an acellular human dermis derived graft, is an example of a commercially available graft that is

[1]Carbon Research Laboratory, University of Dayton Research Institute Dayton, Ohio.
[2]Department of Mechanical Engineering, University of Dayton, Dayton, Ohio.
[3]Center for Tissue Regeneration and Engineering (TREND), University of Dayton, Dayton, Ohio.
[4]Wright Brothers Institute Endowed Chair in Nanomaterials and Chemical and Materials Engineering, University of Dayton, Dayton, Ohio.
[5]Perspective Advantage Solutions, LLC, Dayton, Ohio.
[6]Department of Biology, University of Dayton, Dayton, Ohio.

commonly utilized in surgery for soft tissue augmentation and repair.[4,10–13] The elastic properties of skin-derived scaffolds make GraftJacket (GJ) an inferior replacement for stiffer tissues such as tendon. Hence current limitations in tissue processing has spawned interest in emerging technologies that enable precise engineering and manufacturing of scaffold materials on a nanoscale that recapitulate the unique mechanical needs of a variety of tissues while promoting tissue repair that also occurs on a nanoscale (Table 1).

To date, biomedical scaffold materials have included synthetic, semi-synthetic, and tissue derived matrices with or without biologic activity from growth factors or living cells incorporated within the scaffolds.[10,14–19] Various extracellular matrix molecules such as collagen and resorbable synthetic materials commonly utilized in suture and medical implants have all been employed as scaffolds in the past.[16,18,20,21] The most advanced generations of commercially available scaffolds attempt to provide some level of structural function with biologic activity such as Trinity® (Orthofix),[22] which combines mesenchymal stem cells with a cancellous bone allograft that is utilized for bone healing, Infuse® (Medtronic),[23] which incorporates recombinant bone morphogenic protein-2 with a resorbable collagen scaffold sponge is utilized in spine fusion, Apligraf® (Organogenesis),[24] which integrates human keratinocytes and dermal fibroblasts with bovine type I collagen as a graft for the treatment of skin ulcerations, and GJ Matrix,[4] an acellular human dermis derived scaffold with retained growth factors and extracellular matrix molecules.

Carbon-based materials are novel subsets of synthetic materials that have been incorporated in medical scaffolds, implants, and nanoartifact drug delivery vehicles because of their strength, flexibility, durability, and biocompatibility but have been examined less extensively as a combined vehicle for cell delivery and biomechanical construct for soft tissue repair and regeneration.[25–30] Potential advantages of an engineered carbon scaffold may include the following: (i) tunable geometric and surface characteristics to fit biologic demands of a healing tissue (ii) reproducible mechanical properties to meet specific functional requirements (iii) lack of donor site morbidity (iv) no communicable disease transmission (v) unlimited availability.

The current study examined the mechanical behavior of two fibrous carbon-based scaffolds and evaluated their potential as a vehicle for cell and biologics delivery that promotes tissue repair. The structure, tensile properties, and human fibroblast adhesion and proliferation on carbon scaffold substrates were analyzed and compared to a control scaffold, GJ Matrix, which is commonly utilized in surgery for soft tissue augmentation and repair.[4,6,10,11,13,31,32]

Materials and Methods

Materials

A spool of commercially available PAN-based carbon fibers from Cytec Industries, Inc. was used to create carbon scaffold substrates. Before scaffold preparation, carbon fibers were heat treated at 150°C for 30 min and milled to 5 mm size. A 1% (weight/volume) polycaprolactone (PCL)/acetone solvent was added to form a slurry. The slurry was cast in a mold and evaporated to leave behind a veil scaffold (labeled carbon veil 1 [CV1] and CV2, $n=10$/group). Unidirectional carbon laminate was made by aligning unidirectional P120 carbon tow (labeled carbon fabric 1 [CF1] and CF2, $n=10$/group). Samples were ultrasonicated and sterilized in 100% ethanol for 1 h. GJ Matrix ($n=20$) were donated by Wright Medical Technology, Inc.

Environmental scanning electron microscopy of scaffolds

Environmental scanning electron microscopy (ESEM) was used to examine geometric properties of scaffolds. A Hitachi ESEM (Hitachi) was used to visualize the microscale surface of scaffolds. Samples were imaged at 500×.

Micro-computed tomography of scaffolds

Micro-computed tomography (labeled μCT; Scanco Medical) was used to analyze scaffold porosity, pore size, and scaffold geometry. Samples were analyzed before mechanical testing and culture. Samples were scanned at a resolution of 7 μm/slice. Sample porosity was calculated with proprietary software provided by Scanco Medical.

Mechanical characterization of scaffolds

Tensile properties of scaffolds were examined using a MTS mechanical tester (MTS). Grip fixtures were utilized to secure samples and prevent sample tearing. All scaffolds were hydrated when tested under tension as GJ function *in vivo* is under hydrated conditions. Hydration of GJ and carbon scaffolds were performed according to manufacturer instructions for GJ hydration. Ten samples for each scaffold group were analyzed at 25.4 mm/min. Stress and strain data were recorded. The slope of the linear region of the stress/strain curve was used to determine the elastic modulus. For this study, the strain region between 0% and 3% was considered low strain, for comparison of carbon-based scaffolds to GJ control.

Fibroblast culture on scaffolds

Human dermal fibroblasts (ATCC CRL2703) were cultured in flasks with Dulbecco's F12 medium (Gibco BRL, Invitrogen) supplemented with 10% fetal bovine serum (FBS; Atlanta Biologicals) and 1% penicillin/streptomycin (100 U/100 mg per mL; Gibco BRL, Invitrogen), for simplicity labeled (complete media). Cells were incubated at 37°C in 5% CO_2 with 100% humidity. Fibroblasts from 5–8 passages were used for all cell studies.

Morphometric analysis of fibroblast growth on scaffolds

Fibroblast morphology was characterized after 12, 48, and 96 h of cell culture on scaffolds using fluorescent microscopy. Samples were rinsed twice with sterile phosphate-buffered saline (PBS) to remove nonattached debris. Cells were then fluorescently labeled with 20 mM Rhodamine phalloidin to identify polymerized actin (Invitrogen) and 20 mM 4′,6-diamidino-2-phenylindole (DAPI) nuclear counterstain (Invitrogen) to identify the cell nucleus. Scaffolds were then rinsed in PBS to clear excess label. Cell fluorescence was preserved with Prolong Gold reagent (Invitrogen). Cell fluorescence and morphology were characterized at a magnification range from 10× to 40×.

Fibroblast viability in scaffold cultures

Multiple methods were used to quantify cell adhesion and proliferation. Carbon and GJ scaffolds (area: 25mm^2) were placed in 100 mm^2 round tissue culture dishes ($n=10$/experimental group). Fibroblasts (60,000 cells/sample) were seeded onto scaffold samples in 200 μL aliquots of F12 complete media containing 10% FBS (300,000 cells/mL) and placed into the incubator at 37°C, 5% CO_2, and 100% humidity. After 12 h, samples were moved to 24-well plates, retaining only cells attached to the scaffolds, and 2 mL of complete media was added to each well and returned to the incubator. Growth media was changed every second day. Scaffolds were immediately processed for biochemical characterization as described below to measure cell attachment. To characterize fibroblast proliferation, cell seeded scaffolds were cultured in 2 mL of complete media for a period of 12, 48, and 96 h before analysis.

Cell attachment and proliferation was quantified with fluorescence microscopy and WST-1 biochemical assay (Roche Scientific) at 12, 48, and 96 h cultures. Cell adhesion to scaffold surfaces was quantified by counting cell nuclei labeled with DAPI at each culture time point. For each scaffold, five images were acquired, spanning the entire length of the sample. Fibroblasts were imaged and nuclei were counted using Metamorph software package (Molecular Devices).

Concurrently, cell viability was assessed at 12, 48, and 96 h using WST-1 assay. The tetrazolium salt 2-(4-iodophenyl)-3-(4-nitrophenyl)-5-(2,4-disulfophenyl)-2H-tetrasolium, better known as WST-1, was used to quantify viable fibroblasts in culture. Photometric quantification of viable cells was performed by measuring absorbance at 450 and 690 nm using a microplate reader. Cell proliferation was measured as a function of absolute absorbance values (absorbance at 450 nm–absorbance at 690 nm). Fibroblast growth in wells without scaffolds was used as a positive control while scaffolds without seeded cells were used as negative controls. Nonspecific absorbance from media and scaffold samples was subtracted from absorbance readings. Absorbance values were compared to control values and directly related to cell viability.

Statistical analysis

Statistical analyses were performed using SPSS Statistics 19 Software Package (SPSS, Inc.). All experimental results were statistically evaluated using one-way analysis of variance, with $p<0.05$ indicating significant differences among experimental groups. *Post hoc*, multiple comparison analyses were also performed using the Tukey-Kramer test. Multivariate stepwise linear regression was carried out to model the relationship between experimental parameters (porosity, elastic modulus, stress, and thickness) and load failure of carbon scaffolds and GJ. Additionally, linear regression was performed to model the relationship between scaffold porosity and elastic modulus. Carbon samples were pooled for an n of 40. GJ data was also pooled for data analysis for an n of 20.

Results

Scaffold characterization

As shown in Figure 1, at low magnification (2×), all samples demonstrated porous characteristics, however, GJ was less porous than carbon scaffolds (Fig. 1). This was most apparent with ESEM imaging shown in Figure 2. GJ also displayed two distinct textured sides that relate to the natural stratification of structures in the human dermis (Fig. 2). The deeper dermal side was characterized by an extensive vascular network and was more porous than the more superficial epidermal side of GJ control. GJ demonstrated less continuity and consistency in physical characteristics than engineered carbon in accordance with natural variations typically observed in living tissues but not observed with highly engineered scaffolds such as carbon (Fig. 1). Microscale porosity was examined in all scaffolds by μCT (Fig. 2). Scaffold porosity was most uniform in carbon engineered scaffolds while GJ demonstrated inconsistent porosity attributes hallmarked by regions of large defects up to 1 mm size

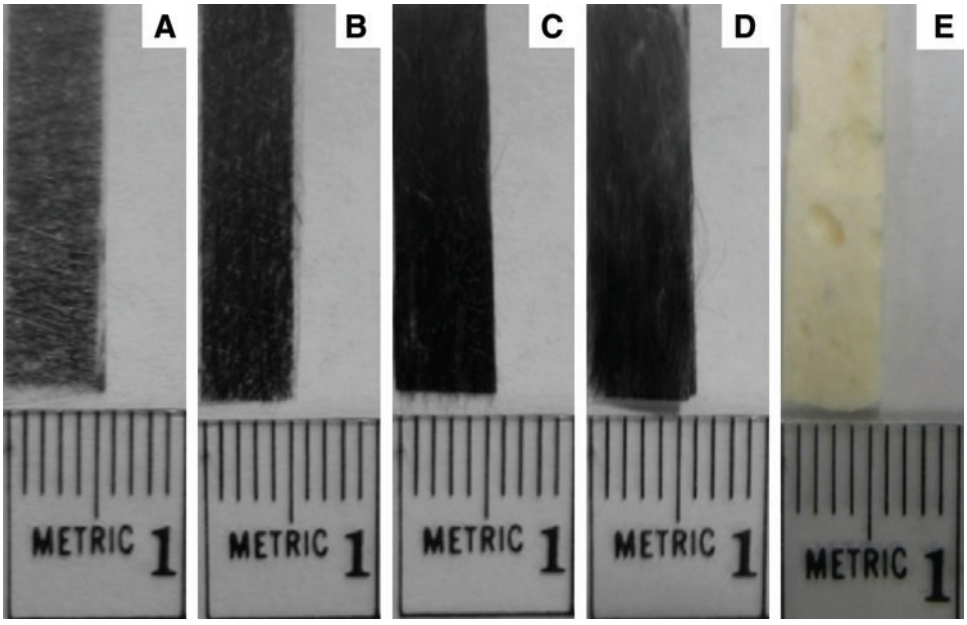

FIG. 1. Low magnification (2×) images of carbon veil (CV), carbon fabric (CF), and GraftJacket® (GJ) control scaffolds. **(A)** CV1; **(B)** CV2; **(C)** CF1; **(D)** CF2; **(E)** GJ. GJ control displayed large volume defects throughout the scaffold. Color images available online at www.liebertonline.com/tea

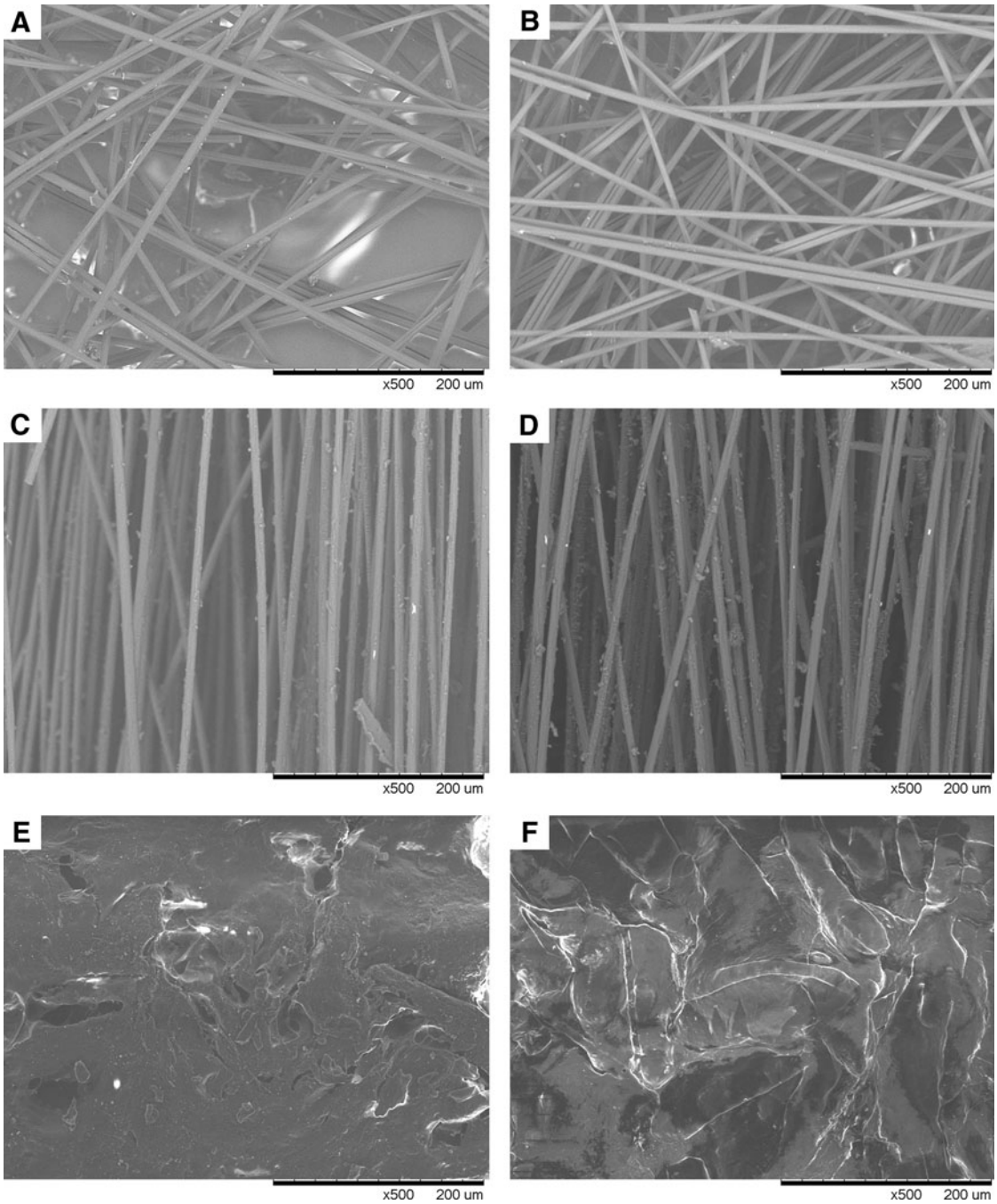

FIG. 2. Environmental scanning electron microscopy images of CV, CF, and GJ scaffolds. **(A)** CV1; **(B)** CV2; **(C)** CF1; **(D)** CF2; **(E)** GJ epidermal surface; **(F)** GJ dermal surface.

that were not observed in any carbon engineered scaffolds (Fig. 2). GJ control displayed a closed porosity of (35%), whereas carbon scaffolds showed an open cell structure (CF1 and 2: 55% and 70%, respectively; CV1 and 2: 80% and 95%, respectively) (Fig. 2 and Table 2). Structural characterization of scaffolds demonstrated less variability in porosity of carbon scaffolds compared with GJ, as indicated by smaller average standard deviations in porosity measurements. The standard deviation of carbon scaffold porosity was approximately 75% smaller than GJ (Table 2). CF1 and CF2 exhibited greater unidirectional fiber orientation, while CV1 and CV2 scaffolds consisted of more randomly organized fibers (Figs. 2 and 3).

Mechanical behavior of carbon scaffolds

The mechanical properties of scaffolds were tested under tension. As shown in the magnified low strain range (0%–3%) GJ displayed a smaller stress-strain ratio compared to carbon-based scaffolds (Fig. 4). This is consistent with deformation characteristics commonly observed in the "toe region" of biological tissues. Further, as is displayed by the gradual decrease

Table 1. Published Mechanical Properties of Biological Tissues

	Maximum load (N)	*Maximum stress (MPa)*	*Maximum strain (%)*	*Elastic modulus (MPa)*
Femur[a]	111.0 ± 11.9	131 ± 13	5.00 ± 1.2	16,600 ± 174
Anterior cruciate ligament[b]	1627 ± 491	26.8 ± 9.1	28.5 ± 9.1	109.00 ± 50.0
Superior infraspinatus tendon[c]	462.8 ± 237	14.6 ± 7.7	NA	120.00 ± 53.1

[a]Fung (1993).[51]
[b]Holzapfel and Ogden (2006).[52]
[c]An (2000).[53]
NA, data not published.

in the slope of the curve, GJ exhibited longer strain regions with a yielding behavior and no catastrophic failure (Fig. 4). Conversely, carbon scaffolds carried more load and handled a larger stress at lower strain and catastrophically failed. From a load failure perspective, CF1 displayed the greatest strength, with a maximum load of 56 ± 4 N and was significantly greater than other carbon scaffolds and GJ control. CF2 and GJ were most similar (27 ± 4 N and 36 ± 16 N) without statistically significant differences in load failure ($p > 0.05$) (Table 2; Fig. 5). On the other hand, CV1 and CV2 scaffolds exhibited significantly lower ($p = 0.01$) maximum loads (3 ± 0.2 N and 4 ± 0.2 N), than both CF scaffolds and GJ control (Table 2; Fig. 5). Results also showed that CF1 displayed a significantly greater ($p = 0.005$) maximum stress (21 ± 0.9 MPa) as compared with GJ control (15 ± 2.5 MPa) (Table 2; Fig. 6). The variability of load failure and porosity was much greater in GJ controls than engineered carbon scaffolds, as demonstrated by higher standard deviations of test measurements. Additionally, all carbon-engineered scaffolds (CV1, CV2, CF1, CF2) displayed significantly greater ($p = 0.005$) elastic modulus values (860 ± 45, 910 ± 47, 995 ± 83, and 835 ± 66, respectively) than GJ control (Table 2; Fig. 6).

Cytoskeletal actin polymerization and morphology of fibroblasts cultured on carbon scaffolds

Cell density and morphology of fibroblasts cultured on scaffolds were characterized using fluorescent microscopy (Fig. 7). Actin filament organization was most distinct in elongated fibroblasts, which grew in a collinear pattern along carbon fibers. This pattern of fibroblast growth was most prevalent in CV, which was notably more porous than other tested scaffolds. Actin polymerization was diffuse and without distinct actin filament formation in fibroblasts with a round morphology and in fibroblasts observed in clusters. This pattern of morphology was most prevalent in regions of dense carbon fiber arrangement more frequently observed in CF than CV where CF fibers were arranged in a tightly packed parallel alignment (Fig. 2). Although round and elongated fibroblast morphology could be observed in all scaffolds, predominant patterns of morphology suggest that cell aggregation and round morphology may be more related to the density of carbon fiber distribution rather than differences between parallel and divergent fiber orientation within carbon scaffolds.

Cell adhesion and proliferation exhibited two distinct growth patterns in GJ controls that were specific to the epidermal and dermal surfaces of GJ. The dermal surface of GJ controls supported cell adhesion and growth with extensive filamentous actin organization in fibroblasts while the epidermal surface supported minimal actin polymerization in fibroblasts (Fig. 7). The morphology of fibroblast adhesion and growth on CF scaffolds closely resembled that of fibroblast adhesion to the epidermal surface of GJ controls where extensive actin polymerization could be identified in fibroblasts (Fig. 7). The morphology of fibroblast adhesion to CV scaffolds more closely resembled fibroblast adhesion to the dermal surface of GJ controls (Fig. 7).

Fibroblast adhesion and proliferation on carbon scaffolds

Cell density and viability assays were conducted to assess fibroblast growth and proliferation on carbon scaffolds. The cell density of fibroblasts cultured on scaffolds for periods of 12, 48, and 96 h was determined using Metamorph counting software. Fibroblast adhesion and proliferation on CF and CV scaffolds was significantly lower than growth on GJ controls ($p < 0.01$) (Fig. 8). Total fibroblast adhesion to CF1 was significantly greater than CV scaffolds ($p = 0.005$) (Fig. 8). There were significant differences in cell adhesion ($p = 0.01$) and proliferation ($p = 0.005$) between CF1 and CF2 scaffold cultures. Further, there was a positive proportional trend in fibroblast adhesion to scaffolds with lower porosity (Fig. 8).

Table 2. Material Properties of Carbon Veil, Carbon Fabric, and GraftJacket® Control Scaffolds

	Density (g/cm^3)	*Porosity (%)*	*Thickness (mm)*	*Maximum load (N)*	*Maximum stress (MPa)*	*Maximum strain (%)*	*Elastic modulus (MPa)*
CV1	0.50	95 ± 1.0**	0.30 ± 0.03	3.0 ± 0.20**	2.5 ± 0.10***	3.3 ± 0.20***	860 ± 45**
CV2	0.60	80 ± 4.0**	0.32 ± 0.02	4.0 ± 0.20**	3.2 ± 0.20***	2.5 ± 0.20***	910 ± 47**
CF1	0.80	55 ± 9.0	0.43 ± 0.03	56 ± 4.0*	21 ± 0.90**	2.3 ± 0.10**	995 ± 83**
CF2	0.70	70 ± 7.0*	0.42 ± 0.03	27 ± 3.0*	16 ± 1.0	2.7 ± 0.20**	835 ± 66**
GJ	1.1–1.4	35 ± 20	0.48 ± 0.14	36 ± 16	15 ± 2.5	49 ± 13	80 ± 19

Values with an asterisk (*) are significantly different from GJ.
*Significance at $p < 0.05$; **significance at $p \leq 0.005$; ***significance at $p \leq 0.001$.
CV, carbon veil; CF, carbon fabric; GJ, GraftJacket® Matrix.

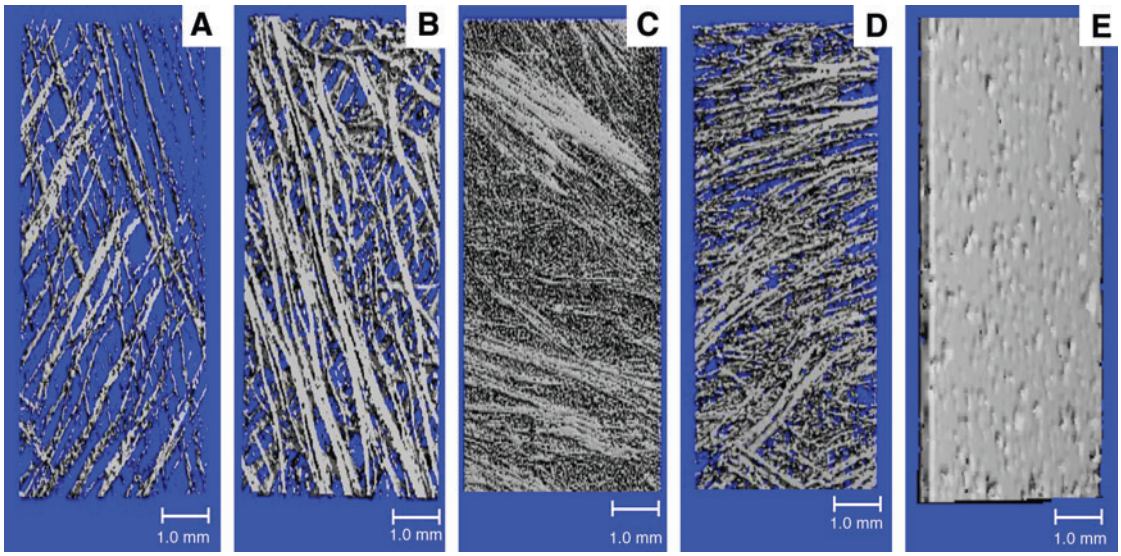

FIG. 3. Micro-computed tomography imaging of CV, CF, and GJ scaffolds. **(A)** CV1; **(B)** CV2; **(C)** CF1; **(D)** CF2; **(E)** GJ. Color images available online at www.liebertonline.com/tea

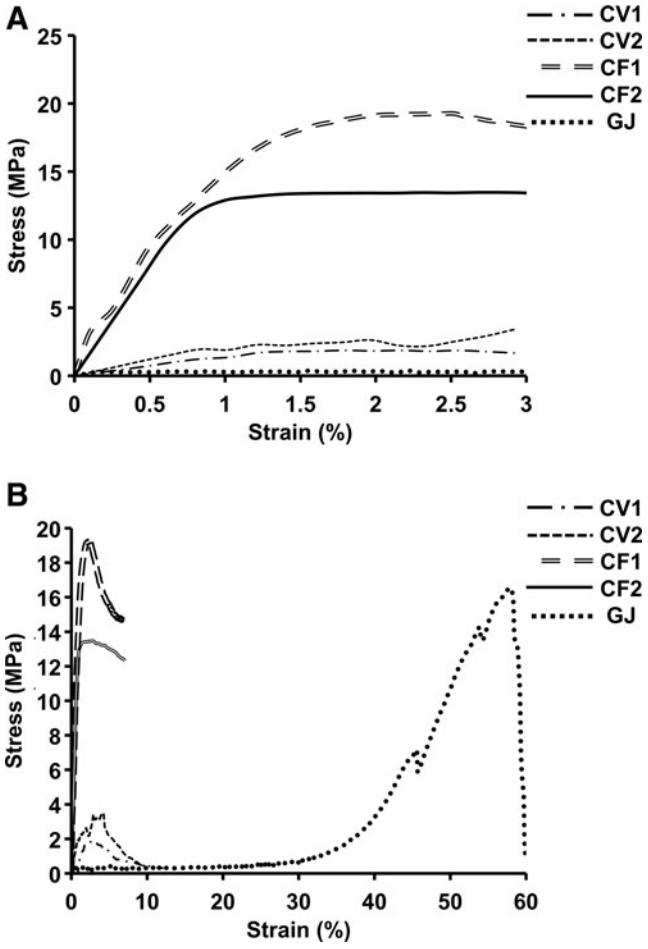

FIG. 4. Mechanical tension testing results for CV, CF, and GJ scaffolds. **(A)** Magnified section of stress and strain region depicts low strain range (0%–3%); **(B)** Stress/strain behavior for experimental scaffolds. Rate of test was 25.4 mm/min.

WST-1 analysis demonstrated marginal differences in fibroblast viability and proliferation on carbon and GJ control scaffolds during the first 12 h of culture, however, significantly higher WST-1 absorbance was measured in dermal control cultures at 96 h which suggests carbon scaffolds were less capable of supporting a high rate of cell proliferation over time ($p=0.01$). At 96 h, CF was most similar to GJ controls in sustaining fibroblast growth with CF1 and CF2 demonstrating 16% and 27% less absorbance than GJ controls. This contrasts CV scaffolds, which showed notably lower capacity to support cell growth than GJ with 80% and 77% less absorbance on CV1 and CV2.

Multivariate stepwise regression

Stepwise regression analysis demonstrated that scaffold thickness and porosity accounted for significant variability in load failure of GJ (Adjusted $R^2=0.787$, Adjusted $R^2=0.924$) but not carbon scaffolds (Table 3). The variability in load

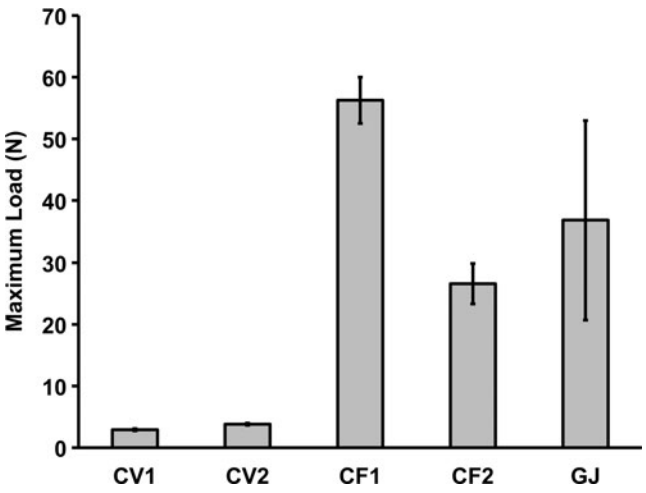

FIG. 5. Maximum load analysis of CV, CF, and GJ scaffolds. Values expressed as mean ± standard deviation (SD).

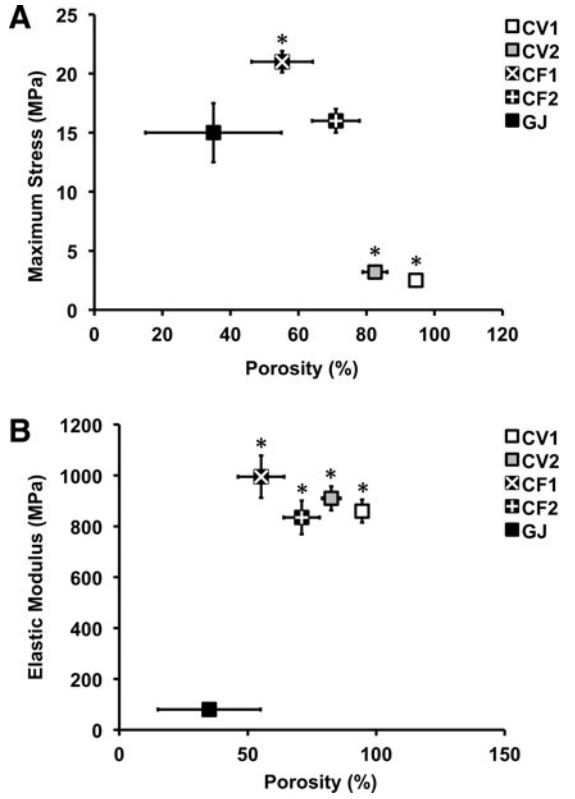

FIG. 6. Comparison of maximum stress and elastic modulus against porosity of CV, CF, and GJ scaffolds. **(A)** Maximum stress against porosity of experimental scaffold samples; **(B)** Elastic modulus against porosity of experimental scaffold samples. Values expressed as mean ± SD. Data points with an asterisk (*) are significantly different from GJ control (Tukey-Kramer $p < 0.01$).

failure of carbon scaffolds was more closely related with modulus and stress properties of carbon (Adjusted $R^2 = 0.924$). Additionally, linear regression analysis revealed that porosity did not strongly correlate with elastic modulus in both control and carbon scaffold groups (Adjusted $R^2 = 0.087$ and Adjusted $R^2 = 0.383$) (Table. 4).

Discussion

Carbon has previously been used in a limited capacity in medical implants used for soft tissue augmentation.[26,27,30,33,34] In the past, researchers have combined biopolymers[35–37] and altered the surface chemistry[38] of materials to optimize the biocompatibility and function of scaffolds. The use of fibrous carbon materials for medical research has steadily grown as processing and characterization methods have become more sophisticated and allow precise tuning of physical and structural properties of carbon-based scaffolds on a nanoscale. The objective of this study was to investigate the potential use of carbon as a biomedical scaffold for the surgical reconstruction of soft tissues with a hypothesis that carbon may provide an optimal balance of biomechanical strength and the capacity to deliver living cells and biologics to surgical sites to promote tissue repair while restoring tissue function. This study demonstrated that carbon may support biologic functions in addition to serving biomechanical functions as a material known for its biocompatibility, durability, and strength.

Cell adhesion and proliferation studies showed that there is little difference between carbon and GJ control's capacity to support early cell adhesion, a critical factor for scaffold integration and healing *in vivo*. This is supported by marginal differences in fibroblast density and viability on both carbon and control scaffolds during short-term *in vitro* cultures at 12 h and up to 48 h in CF cultures. The capacity for carbon to sustain fibroblast adhesion and viability at 96 h culture suggests a potential use of carbon as a scaffold for sustained delivery of growth factors to sites of injury to promote tissue healing such as the commercially available scaffold Apligraf which is composed of a collagen scaffold seeded with keratinocytes and dermal fibroblasts.[24] Fibroblast adhesion to carbon and the capacity to sustain cell growth are critical factors for the use of carbon as a vehicle for delivering viable cells to a region of soft tissue reconstruction where the combination of cells and scaffold are a source of extracellular matrix synthesis, paracrine release of growth factors, and nidus for tissue repair.

Although fibroblast adhesion to carbon and GJ was followed by cell proliferation, proliferation was slower on carbon scaffolds as demonstrated by fewer cells and less metabolic activity measured by WST-1 assays in longer-term cultures of 96 h. These findings suggest significant biologic property differences between carbon and the tissue derived GJ. These differences yielded a higher rate of fibroblast proliferation on GJ than carbon. It is reasonable to speculate that enhanced fibroblast proliferation on GJ was stimulated by residual activities of growth factors such as basic fibroblast growth factor, which has been shown to be retained in GJ but not present in carbon.[6] Hence carbon's limited potential in supporting a high rate of cell proliferation may be due to its lack of a naturally derived tissue factor found in GJ. Further investigation of the specific role of growth factors present in GJ and selective conjugation of growth factors to carbon scaffolds maybe necessary to optimize carbon's potential to promote cell proliferation to levels observed with current tissue scaffolds utilized in surgery today. Recent studies have shown that some synthetic fiber scaffolds can be modified to mimic the activity of specific growth factors such as vascular endothelial growth factor and promote regenerative processes such as neovascularization.[39] This may be an alternate approach to growth factor conjugation to carbon that improves the biologic potential of carbon as a regenerative scaffold.

It is unlikely that lower rates of fibroblast proliferation on carbon scaffolds was due to carbon toxicity as carbon has been shown to be non toxic in itself[17,27,33,40,41] and progressive cell proliferation would not be expected as observed if carbon was cytotoxic. Lower levels of total fibroblast adhesion to carbon scaffolds than GrafJacket may have been a result of geometric differences in the design and structure of carbon and GrafJacket scaffolds. CV, the more porous of the two carbon scaffolds, demonstrated less capacity for cell adhesion and lower proliferation rates as noted by a smaller plateau in WST-1 absorbance and lower levels of cell adhesion than CF and GJ. This is consistent with other studies that demonstrate increased cell proliferation on less porous scaffolds and densely organized regions of carbon fiber organization.[42] These findings are also consistent with literature

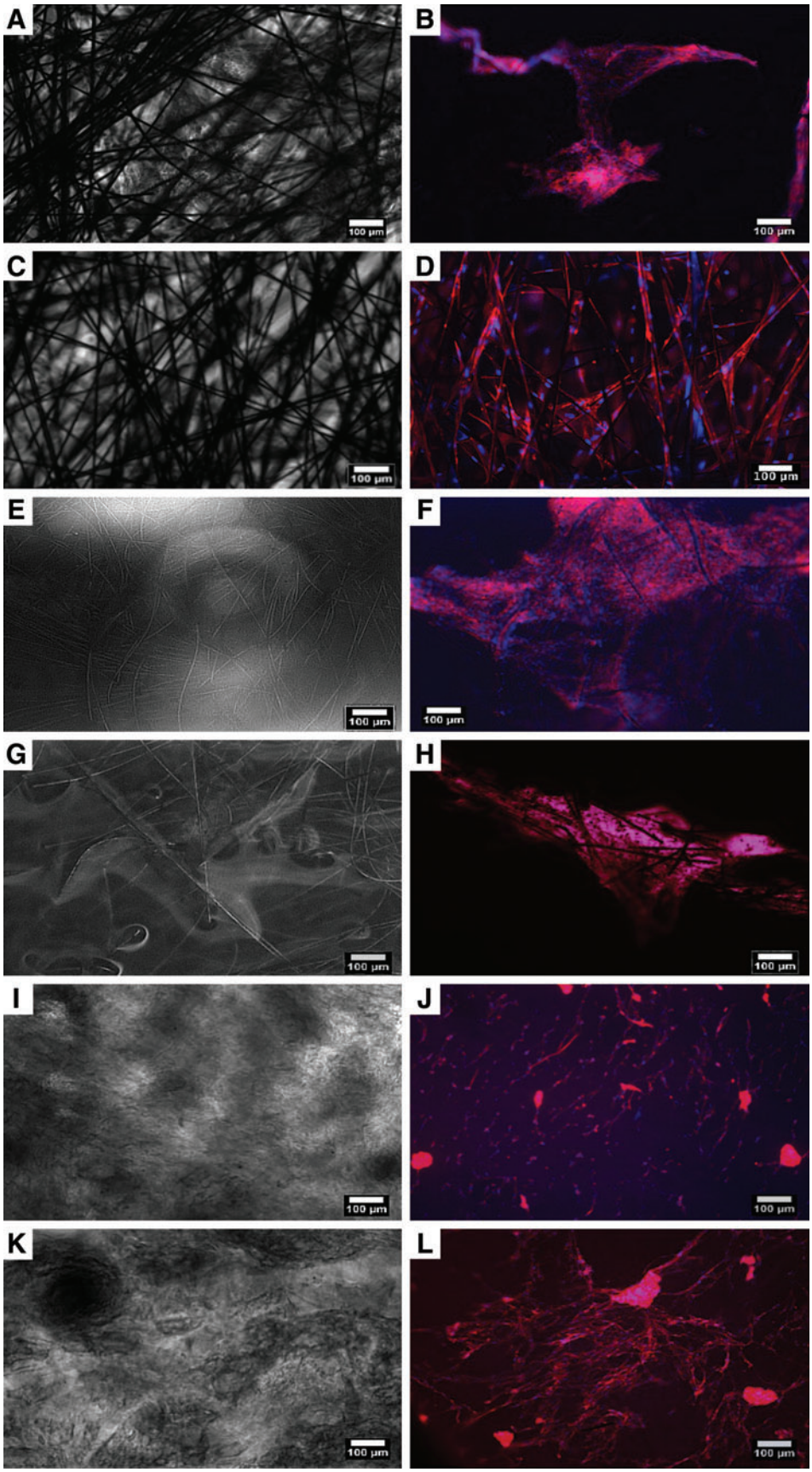

FIG. 7. Phase contrast and fluorescent imaging of fibroblast growth on CV, CF, and GJ scaffold surfaces at 96 h. First column illustrates phase contrast background of scaffold samples. Second column illustrates cellular morphology with polymerized actin labeling (red) and nuclear labeling (blue). **(A)** Phase contrast imaging of fibroblast adhesion to CV1; **(B)** Fluorescence imaging of fibroblast adhesion to CV1; **(C)** Phase contrast imaging of fibroblast adhesion to CV2; **(D)** Fluorescence imaging of fibroblast growth to CV2; **(E)** Phase contrast imaging of fibroblast adhesion to CF1; **(F)** Fluorescence imaging of fibroblast adhesion to CF1; **(G)** Phase contrast imaging of fibroblast adhesion to CF2; **(H)** Fluorescence imaging of fibroblast adhesion to CF2; **(I)** Phase contrast imaging of fibroblast adhesion to the epidermal surface of GJ; **(J)** Fluorescence imaging of fibroblast adhesion to the epidermal surface of GJ; **(K)** Phase contrast imaging of fibroblast adhesion to the dermal surface of GJ; **(L)** Fluorescence imaging of fibroblast adhesion to the dermal surface of GJ. Color images available online at www.liebertonline.com/tea

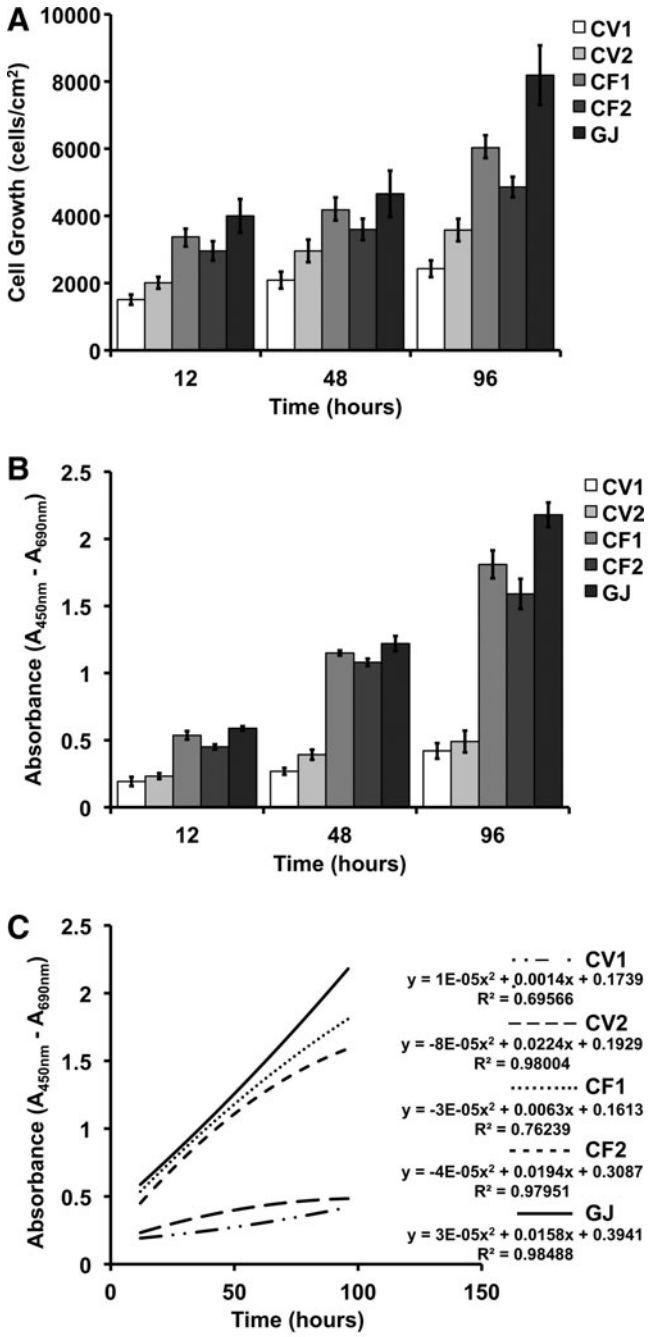

FIG. 8. Quantification of fibroblast growth on CV, CF, and GJ scaffolds. **(A)** Fibroblast quantification on scaffold samples surfaces by cell counting; **(B)** Fibroblast quantification on scaffold surfaces by WST-1 assay absolute absorbance measurement of fibroblast viability; **(C)** Fibroblast proliferation rates on scaffolds based on WST-1 absorbance. Sample size was $n=10$/experimental group. Values expressed as mean ± SD.

regarding cell proliferation on synthetic fibers where cell proliferation was greatest in regions of cell aggregation and spreading.[41,43,44] The carbon fiber used in this study had a high degree of basal planes oriented along the fiber axis. The basal planes are formed during the carbonization step of carbon fiber processing. After carbonization the fibers exhibit a high degree of axial preferred orientation with thick crystallite stacking. As is shown in Figure 7, there was high actin polymerization along the fiber axis and the fiber axis. This material property has been previously shown to promote cell growth.[33,45] The optimal pattern of fiber organization, dimension, and porosity that maximizes the ability of carbon to deliver cells, promote tissue repair, and enable tissue ingrowth and neovascularization needs to be further explored.

Table 3. Multivariate Stepwise Regression Modeling of Carbon Veil, Carbon Fabric, and GraftJacket® Scaffold Load Failure

A. Regression Modeling of Maximum Load Failure of Carbon Scaffolds ($N=40$)

Variable	*B*	*SE B*	β
Step 1			
Stress	2.55	0.117	0.962*
Step 2			
Stress	2.35	0.077	0.886*
Modulus	0.059	0.008	0.229*

$R^2=0.926$ for Step 1; Adjusted $R^2=0.924$ for Step 1, $R^2=0.972$ for Step 2, Adjusted $R^2=$ Adjusted $R^2=0.971$ for Step 2, (*$p<0.01$). Porosity and thickness were removed due to significance test ($p>0.05$).

B. Regression Modeling of Maximum Load Failure of GraftJacket® ($N=20$)

Variable	*B*	*SE B*	β
Step 1			
Porosity	−1.15	0.383	−0.690*
Step 2			
Porosity	−1.28	0.234	−0.764**
Thickness	22.8	5.35	0.596**

$R^2=0.476$ for Step 1; Adjusted $R^2=0.423$ for Step 1, $R^2=0.826$ for Step 2, Adjusted $R^2=0.787$ for Step 2, (*$p<0.05$, **$p<0.01$). Stress and elastic modulus were removed due to significance test ($p>0.05$).

Maximum load failure was tested as the dependent variable with scaffold thickness, porosity, maximum stress, and elastic modulus tested as independent variables. Both nonadjusted and adjusted R^2 values for each regression step are displayed.

B, slope of the regression; SE B, standard error of slope; B/SE B, T statistic from slope.

Table 4. Linear Regression Modeling of Elastic Modulus as a Function of Scaffold Porosity in Carbon Veil, Carbon Fabric, and GraftJacket®

A. Linear Regression Modeling of Elastic Modulus as a Function of Porosity in Carbon Scaffolds ($N=40$)

Variable	*B*	*SE B*	β
Porosity	−3.42	0.681	−0.631*

$R^2=0.399$; Adjusted $R^2=0.383$ (*$p<0.001$).

B. Linear Regression Modeling of Elastic Modulus as a Function of Porosity in GraftJacket® ($N=20$)

Variable	*B*	*SE B*	β
Porosity	−0.409	0.286	−0.412

$R^2=0.170$; Adjusted $R^2=0.087$ ($p>0.05$).

Elastic modulus was tested as the dependent variable with scaffold porosity as independent variable. Both nonadjusted and adjusted R^2 values are displayed.

In the past, it has been exceptionally challenging to engineer synthetic scaffolds or process naturally derived tissues to recapitulate the biologic parameters necessary for tissue repair without compromising the mechanical strength and stiffness of scaffolds. This is a particularly keen problem with scaffolds utilized to repair major tendon injuries of the rotator cuff or Achilles tendon, where dermal scaffolds currently used to augment tissue repair are composed of similar extracellular matrix molecules but fail to restore the elastic properties of tendons.[10,12,14,46–48] Regression modeling demonstrated that scaffold porosity, a major factor influencing graft neovascularization and cell delivery capacity of fibrous scaffolds did not significantly influence the load failure and modulus of carbon but did influence variance in load failure of GJ. These findings suggest design advantages of carbon scaffold engineering that maximize porosity attributes conducive to scaffold neovascularization without compromising the mechanical strength of a scaffold that is needed but often lacking in currently available products. Results of this study demonstrated greater consistency, less variation, and fewer defects in the dimensions, porosity, and thickness of engineered carbon than the commercially available GJ (Fig. 6). The ability to consistently manufacture precise physical and dimensional properties of carbon may further minimize design, biomechanical and manufacturing limitations of current scaffolds used in surgery. Hence achieving the optimal tunable balance between biologic properties and biomechanical function of scaffolds may be technically easier through carbon engineering than developing improved technologies of human tissue processing. The possibility of engineering carbon with mechanical properties of a mature tissue despite its lack of a mature cellular and extracellular matrix provides a potential advantage of carbon over current biologic scaffolds that require prolonged processes of tissue healing, reorganization, and fibrosis to achieve their maximum mechanical strength. This advantage potentially shortens periods of postoperative inactivity in patients as the mechanical strength of tendons repaired with carbon may be restored sooner with surgery without the need for prolonged periods of immobilization to achieve maximal tissue strength. This may ultimately reduce the risk of postoperative morbidity and mortality associated with prolonged periods of inactivity and immobilization by enabling patients to return to unrestricted activities earlier.[49,50]

In summary, carbon may represent an alternative material suitable for future development as a soft tissue substitute that potentially optimizes the biologic and mechanical properties required for a graft product utilized in surgery. Further investigation is required to characterize and model the relationships of biologic, mechanical, and design properties of this material to maximize its potential use as a biomechanical scaffold and vehicle for delivering biologics that promote tissue repair and regeneration.

Acknowledgment

The authors would like to thank Wright Medical, Inc. for donating GJ Matrix samples. The authors would also like to thank the Dayton Area Graduate Studies Institute for supporting this work through a fellowship as well as Dr. Eric Benbow for the use of Endnote® Software.

Disclosure Statement

The authors would also like to disclose that Wright Medical played no role in the design, implementation, data analysis, or interpretation of findings of this study. None of the authors of this article received financial remuneration or compensation for conducting this study. No competing financial interests exist.

References

1. Sheridan, R.L., and Choucair, R.J. Acellular allogenic dermis does not hinder initial engraftment in burn wound resurfacing and reconstruction. J Burn Care and Rehabil **18,** 496, 1997.
2. Sikka, R.S., Narvy, S.J., and Vangsness, C.T. Anterior cruciate ligament allograft surgery underreporting of graft source, graft processing, and donor age. Am J Sports Med **39,** 649, 2011.
3. Azar, F.M. Tissue processing: role of secondary sterilization techniques. Clin Sports Med **28,** 191, 2009.
4. Cornwell, K.G., Landsman, A., and James, K.S. Extracellular matrix biomaterials for soft tissue repair. Clin Podiatr Med Surg **26,** 507, 2009.
5. Billiar, K., Murray, J., Laude, D., Abraham, G., and Bachrach N. Effects of carbodiimide crosslinking conditions on the physical properties of laminated intestinal submucosa. J Biomed Mater Res **56,** 101, 2001.
6. Valentin, J.E., Badylak, J.S., McCabe, G.P., and Badylak, S.F. Extracellular matrix bioscaffolds for orthopaedic applications—a comparative histologic study. J Bone Joint Surg Am **88A,** 2673, 2006.
7. Bjork, J.W., Johnson, S.L., and Tranquillo, R.T. Ruthenium-catalyzed photo cross-linking of fibrin-based engineered tissue. Biomaterials **32,** 2479, 2011.
8. Scutt, N., Rolf, C.G., and Scutt A. Tissue specific characteristics of cells isolated from human and rat tendons and ligaments. J Orthop Surg Res **3,** 32, 2008.
9. MacLeod, T.M., Williams, G., Sanders, R., and Green, C.J. Prefabricated skin flaps in a rat model based on a dermal replacement matrix Permacol (TM). Br J Plast Surg **56,** 775, 2003.
10. Barber, F.A., McGarry, J.E., Herbert, M.A., and Anderson, R.B. A biomechanical study of Achilles tendon repair augmentation using GraftJacket matrix. Foot Ankle Int **29,** 329, 2008.
11. Snyder, S.J., Arnoczky, S.P., Bond, J.L., and Dopirak R. Histologic evaluation of a biopsy specimen obtained 3 months after rotator cuff augmentation with GraftJacket matrix. Arthroscopy **25,** 329, 2009.
12. Lee, D.K. A preliminary study on the effects of acellular tissue graft augmentation in acute Achilles tendon ruptures. J Foot Ankle Surg **47,** 8, 2008.
13. Wong, I., Burns, J., and Snyder S. Arthroscopic GraftJacket repair of rotator cuff tears. J Shoulder Elbow Surg **19,** 104, 2010.
14. Ozaki, J., Fujimoto, S., Masuhara, K., Tamai, S., and Yoshimoto S. Reconstruction of chronic massive rotator cuff tears with synthetic materials. Clin Orthop Relat Res **202,** 173, 1986.
15. Brown, B.N., Barnes, C.A., Kasick, R.T., Michel, R., Gilbert, T.W., Beer-Stolz, D., *et al.* Surface characterization of extracellular matrix scaffolds. Biomaterials **31,** 428, 2010.
16. Asran, A.S., Henning, S., and Michler, G.H. Polyvinyl alcohol-collagen-hydroxyapatite biocomposite nanofibrous scaffold: Mimicking the key features of natural bone at the nanoscale level. Polymer **51,** 868, 2010.
17. Demmer, P., Fowler, M., and Marino, A.A. Use of carbon-fibers in the reconstruction of knee ligaments. Clin Orthop Relat Res **271,** 225, 1991.

18. Cornwell, K.G., and Pins, G.D. Enhanced proliferation and migration of fibroblasts on the surface of fibroblast growth factor-2-loaded fibrin microthreads. Tissue Eng Part A **16,** 3669, 2010.
19. Cooper, J.A., Lu, H.H., Ko, F.K., Freeman, J.W., and Laurencin, C.T. Fiber-based tissue-engineered scaffold for ligament replacement: design considerations and *in vitro* evaluation. Biomaterials **26,** 1523, 2005.
20. Freeman, J.W., Woods, M.D., Cromer, D.A., Ekwueme, E.C., Andric, T., Atiemo, E.A., *et al.* Evaluation of a hydrogel-fiber composite for ACL tissue engineering. J Biomech **44,** 694, 2011.
21. Tay, B.Y., Zhang, S.X., Myint, M.H., Ng, F.L., Chandrasekaran, M., and Tan LKA. Processing of polycaprolactone porous structure for scaffold development. Journal of Mater Proc Tech **182,** 117, 2007.
22. Rush, S.M., Hamilton, G.A., and Ackerson, L.M. Mesenchymal stem cell allograft in revision foot and ankle surgery: A clinical and radiographic analysis. J Foot Ankle Surg **48,** 163, 2009.
23. McKay, W., Peckham, S., and Badura J. A comprehensive clinical review of recombinant human bone morphogenetic protein-2 (INFUSE® Bone Graft). Intern Orthop **31,** 729, 2007.
24. Falanga, V., and Sabolinski M. A bilayered living skin construct (APLIGRAF®) accelerates complete closure of hard-to-heal venous ulcers. Wound Repair Regen **7,** 201, 1999.
25. Takaseya, T., Fumoto, H., Shiose, A., Arakawa, Y., Rao, S., Horvath, D.J., *et al. In vivo* biocompatibility evaluation of a new resilient, hard-carbon, thin-film coating for ventricular assist devices. Artif Organs **34,** 1158, 2010.
26. Chen, L., Yuan, X.B., Sun, H.W., Chen, M.Z., Zhao, D.B., Yu, D., *et al. In vivo* study of carbon artificial femoral head. High-Performance Ceramics **434,** 613, 2010.
27. Cao, N., Wang, Q.X., Dung, J.W., Hao, G.Z., and Li, M.S. Characterization and biological behavior of a carbon fiber/carbon composite scaffold with a porous surface for bone tissue reconstruction. New Carbon Mater **25,** 232, 2010.
28. Kettunen, J., Makela, A., Miettinen, H., Nevalainen, T., Heikkila, M., Tormala, P., *et al.* Fixation of distal femoral osteotomy with an intramedullary rod: Early failure of carbon fibre composite implant in rabbits. J Biomat Sci Polym Ed **10,** 715, 1999.
29. Hilder, T.A., and Hill, J.M. Carbon nanotubes as drug delivery nanocapsules. Curr Appl Phys **8,** 258, 2008.
30. Bianco, A., Kostarelos, K., and Prato M. Applications of carbon nanotubes in drug delivery. Curr Opin Chem Biol **9,** 674, 2005.
31. Martin, B.R., Sangalang, M., Wu, S., and Armstrong, D.G. Outcomes of allogenic acellular matrix therapy in treatment of diabetic foot wounds: an initial experience. Int Wound J **2,** 161, 2005.
32. Liden, B.A., and Simmons M. Histologic Evaluation of a 6-Month GraftJacket matrix biopsy used for Achilles tendon augmentation. J Am Podiatr Med Assoc **99,** 104, 2009.
33. Czarnecki, J.S., Lafdi, K., and Tsonis, P.A. A novel approach to control growth, orientation, and shape of human osteoblasts. Tissue Eng Part A **14,** 255, 2008.
34. Baquey, C., Bordenave, L., More, N., Caix, J., and Bassecathalinat B. Biocompatibility of carbon carbon materials—blood tolerability. Biomaterials **10,** 435, 1989.
35. Edwards, S.L., Werkmeister, J.A., and Ramshaw JAM. Carbon nanotubes in scaffolds for tissue engineering. Expert Rev Med Devices **6,** 499, 2009.
36. Fu, T., Zhao, J.L., Wei, J.H., Han, Y., and Xu, K.W. Preparation of carbon fiber fabric reinforced hydroxyapatite/epoxy composite by RTM processing. J Mater Sci **39,** 1411, 2004.
37. Hirata, E., Uo, M., Takita, H., Akasaka, T., Watari, F., and Yokoyama A. Development of a 3D collagen scaffold coated with multiwalled carbon nanotubes. J Biomed Mater Res B-Appl Biomater **90B,** 629, 2009.
38. Chu, P.K. Enhancement of surface properties of biomaterials using plasma-based technologies. Surface Coatings Tech **201,** 8076, 2007.
39. Igarashi, S., Tanaka, J., and Kobayashi H. Micro-patterned nanofibrous biomaterials. J Nanosci Nanotechnol **7,** 814, 2007.
40. Price, R.L., Ellison, K., Haberstroh, K.M., and Webster, T.J. Nanometer surface roughness increases select osteoblast adhesion on carbon nanofiber compacts. J Biomed Mater Res A **70A,** 129, 2004.
41. Morris, D.M., Hindman, J., and Marino, A.A. Repair of fascial defects in dogs using carbon fibers. J Surg Res **80,** 300, 1998.
42. Desai, V.V., and Newman, J.H. The histology of regenerated tissue after failed carbon fibre matrix implants. Knee **6,** 229, 1999.
43. Rajzer, I., Menaszek, E., Bacakova, L., Rom, M., and Blazewicz M. *In vitro* and *in vivo* studies on biocompatibility of carbon fibres. J Mater Sci Mater Med **21,** 2611, 2010.
44. Rnjak, J., Li, Z., Maitz, P.K.M., Wise, S.G., and Weiss, A.S. Primary human dermal fibroblast interactions with open weave three-dimensional scaffolds prepared from synthetic human elastin. Biomaterials **30,** 6469, 2009.
45. Bacakova, L., Svorcik, V., Rybka, V., Micek, I., Hnatowicz, V., Lisa, V., *et al.* Adhesion and proliferation of cultured human aortic smooth muscle cells on polystyrene implanted with N+, F+ and Ar+ ions: Correlation with polymer surface polarity and carbonization. Biomaterials **17,** 1121, 1996.
46. Lee, D.K. Achilles tendon repair with acellular tissue graft augmentation in neglected ruptures. J Foot Ankle Surg **46,** 451, 2007.
47. Branch, J.P. A Tendon graft weave using an acellular dermal matrix for repair of the Achilles tendon and other foot and ankle tendons. J Foot Ankle Surg **50,** 257, 2011.
48. Derwin, K.A., Codsi, M.J., Milks, R.A., Baker, A.R., McCarron, J.A., and Iannotti, J.P. Rotator cuff repair augmentation in a canine model with Use of a Woven Poly-L-Lactide Device. J Bone Joint Surg Am **91A,** 1159, 2009.
49. Cogo, A., Bernardi, E., Prandoni, P., Girolami, B., Noventa, F., Simioni, P., *et al.* Acquired risk factors for deep-vein thrombosis in symptomatic outpatients. Arch Intern Med **154,** 164, 1994.
50. Roberts, C.S., Ojike, N.I., Bhadra, A.K., and Giannoudis, P.V. Venous thromboembolism in shoulder surgery: a systematic review. Acta Orthop Belg **77,** 281, 2011.
51. Fung, Y. Biomechanics: Mechanical Properties of Living Tissues. New York: Springer-Verlag, 1993.
52. Holzapfel, G., and Ogden, R. Mechanics of Biological Tissue. New York: Springer, 2006.
53. An, K.N. Mechanical properties of the posterior rotator cuff. Clin Biomech **15,** 456, 2000.

Address correspondence to:
Jarema Czarnecki, M.S.
Department of Mechanical Engineering
University of Dayton
300 College Park
Dayton, OH 45469

E-mail: jczarnecki1@notes.udayton.edu

Received: September 21, 2011
Accepted: November 17, 2011
Online Publication Date: February 27, 2012